

# Cost-Effective Zinc–Iron Redox Flow Batteries

Subjects: [Energy & Fuels](#)

Contributor: Huan Zhang , Chuanyu Sun , Mingming Ge

Zinc–iron redox flow batteries (ZIRFBs) possess intrinsic safety and stability and have low electrolyte cost. ZIRFB refers to an redox flow batterie (RFB) in which zinc is used as the electrochemically active substance in the electrolyte solutions. The zinc electrode has a reversible anode potential. Zinc ions are stable in both alkaline and acidic environments, even in a neutral electrolyte, and the electrochemical reaction rate is relatively fast.

zinc–iron

redox flow battery

zinc dendrite

energy storage

large scale

carbon electrode

ion exchange membrane

electrolyte design

areal capacity

## 1. Introduction

As a result of the depletion of fossil fuels, the concerns over energy sustainability and environmental issues are given a more and more vital position [\[1\]\[2\]\[3\]\[4\]](#). The power generation of renewable energy, for instance, solar and wind energy, will surely become the main energy sources of future energy strategy. However, the unique intermittence and instability of renewable energy have brought major challenges to the stable operation of the power system, opening temporal and spatial gaps between the consumption of the energy by end-users and its availability, thus, energy storage technology is an effective means that can help achieve stable and efficient renewable energy [\[5\]\[6\]\[7\]](#). Compared with physical techniques (e.g., pumped storage), secondary batteries with higher flexibility have gradually attracted people’s attention [\[8\]\[9\]\[10\]](#). Among the various battery techniques, redox flow batteries (RFBs) have proved to have considerable development potential in large-scale energy storage as a result of their long lifetime, high safety, and high-energy efficiency [\[11\]\[12\]\[13\]\[14\]](#).

According to the electrolyte used, the RFB system mainly includes vanadium-based RFB, iron-based RFBs, zinc-based RFBs, organic RFBs, polysulfide-based RFBs, etc. [\[9\]\[15\]\[16\]\[17\]\[18\]\[19\]\[20\]\[21\]\[22\]](#). To date, the vanadium RFB (VRFB) has become the most mature large-scale energy storage technique, which is suitable for large- and medium-sized energy storage scenarios [\[23\]\[24\]\[25\]\[26\]\[27\]](#). VRFBs have characteristics whose energy efficiency (EE) and cycle life exceed 80% and 200,000 cycles, respectively [\[28\]\[29\]\[30\]\[31\]](#). However, for VRFBs, the cost of vanadium electrolyte accounts for approximately 60% of the battery cost, which greatly increases the initial investment threshold [\[32\]](#). In VRFBs, the adopted acidic electrolyte is prone to corrode the components of the stack, and the choice of the membrane is quite restricted. At present, the Dupont Nafion® is mainly used due to its outstanding chemical stability and proton conductivity. Nevertheless, the high cost of Nafion and vanadium makes VRFBs an expensive energy storage technique among various RFBs.

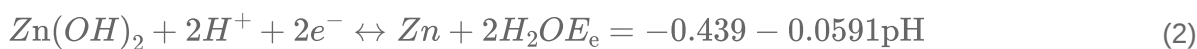
## 2. Characteristics of ZIRFB

### 2.1. The Basic Principle of ZIRFB

Zinc-iron redox flow batteries (ZIRFBs) has the general characteristics of RFBs. That is to say, the ZIRFBs mainly use the changes in the redox state of active substances in the solutions on both sides of the Fe-based cathode and Zn-based anode to realize the charge-discharge process. A ZIRFB is mainly composed of a stack and two electrolyte storage tanks [33]. The electrolyte is stored in a storage tank outside the stack, and then is transported to the inside and outside of the stack by the pump. The redox reaction occurs at the electrodes, and the reactive species flow back to the external storage tank with the electrolyte. The cathode and anode are separated by a separator/membrane, which can optionally allow the supporting electrolyte to pass through to maintain electrolyte balance. The separator/membrane not only separates the half-cells and avoids the cross-mixing of active species, but also provides the required ionic conductivity accompanied by the electrons transfer during the charge-discharge process.

### 2.2. Wide pH Range

Metallic Zn can be electroplated in four various ways with different forms of reactants in the solution depending on the pH from 0 to 16. The relevant reaction equations are as follows:



Unlike other RFBs, the electrolyte of ZIRFB can work in a wide pH range. A higher pH value is conducive to the dissolution and deposition of metallic Zn, despite that the  $\text{Fe}^{2+}/\text{Fe}^{3+}$  redox couple tends to precipitate more easily at high pH. Hence, the appropriate pH range is very important. According to the difference in electrolyte acidity and alkalinity, ZIRFBs are normally divided into three types: alkaline, acidic, and neutral ZIRFBs.

In alkaline ZIRFB, zinc and ferricyanide are used as active substances in the anolyte and catholyte, respectively [34]. The system possesses the electrolyte with relatively low cost and high open-circuit voltage (OCV) of 1.74 V. In the discharge state, the anode side is transformed from Zn to zincate solution (alkaline), while the cathode side ferrocyanide is formed from the previous ferricyanide. When charging, it is the opposite process, which is a reversible reaction compared to the discharge process. However, the cycle performance of the ZIRFB is poor due to the issue of zinc dendrites in the alkaline medium.

In theory, the acidic ZIRFB ( $E_{\text{cell}} = 1.53 \text{ V}$ ) can have a higher energy density [35]. However, in the acidic ZIRFB, the excessive acidity of the solution will affect the deposition of zinc and the hydrolysis of the  $\text{Fe}^{2+}/\text{Fe}^{3+}$  pair, thus, the hydrogen evolution reaction (HER) is prone to occur. For an acidic system with HAc/NaAc as the buffer solution to keep the pH value of the negative electrolyte between 2–6, a high CE (coulombic/current efficiency) can be realized [36].

Compared with alkaline and acidic systems, the neutral ZIRFB system ( $E_{\text{cell}} = 1.43 \text{ V}$ ) is mild and non-corrosive, which has lower requirements for the membrane/separator and other components [37]. The neutral ZIRFB has a lower battery cost than the other two systems, to a certain extent. Nevertheless, regarding the neutral ZIRFB system, it also has to be taken into account that the hydrolysis of  $\text{Fe}^{\text{n}+}$  ions may lead to the decline of battery cycle performance, which is one of the primary challenges for this type of battery.

## 2.3. Zinc Dendrites

In comparison to other battery systems, for instance, lead-based and lithium-based batteries, the capacity/energy/power of the liquid–liquid RFBs can be designed independently [33][38][39]. In fact, the ZIRFB is a kind of “half-RFB”. In the electrode reaction, the iron-based active substance on the cathode side is always present in ionic form, while the zinc-based active substance on the anode side is under the plating–stripping process of zinc. This indicates that the power and capacity of the ZIRFBs are not devised flexibly in comparison with the liquid–liquid RFB because the capacity of the ZIRFB is restricted by the surface area of the electrode during the plating–stripping process [40].

The essential problem during the plating-stripping transversion is that the zinc dendrites mainly formed during battery charging. The existence of zinc dendrites can easily lead to problems such as a reduction in battery coulombic efficiency (CE) and capacity, and the shortening of battery life. In severe cases, it will impale the separator/membrane and lead to a battery short-circuit.

The primary reason is that Zn dendrites are more grievous when the operating current density is high. Under higher current densities, the concentration of zincate or  $\text{Zn}^{\text{n}+}$  in the electrode interface area is extremely low, as the transfer rate of zincate or zinc ions in the electrolyte is obviously slower compared to the reaction rate on the electrode. This may bring about severe concentration polarization [40]. Furthermore, the diffusion of zincate/ $\text{Zn}^{\text{n}+}$  tends to realize on the protrusions of the electrode compared to the flat surface, making it easier for zincate or zinc ions to undergo a plating process on the protrusions, and further results in the generation of Zn dendrites. Due to

the presence of severe zinc dendrites at high operating current densities, ZIRFB usually operates at relatively lower current densities.

## 2.4. Fe(III) Hydrolysis

The hydrolytic reactions of  $\text{Fe}^{3+}$  are much stronger than those of  $\text{Fe}^{2+}$  and, consequently, hydrolysis occurs at a much lower pH. There are few reliable investigations of the hydrolytic reactions of  $\text{Fe}^{2+}$  because of both the low solubility and its propensity to be oxidised to  $\text{Fe}^{3+}$ , which can greatly interfere with the ability to measure  $\text{Fe}^{2+}$  hydrolysis reactions. There have been several investigations that have examined the hydrolytic reactions of  $\text{Fe}^{3+}$ , particularly that of the monomeric species,  $\text{FeOH}^{2+}$ . It is surprising, therefore, to find that a substantial amount of conjecture remains which concerns the stability of the  $\text{Fe}^{3+}$  hydrolytic species and phases [41]. The hydrolysis reaction of  $\text{Fe}^{3+}$  can be described by Reactions (5)–(7) [41]. Similar to standard hydrolysis reactions, the interaction of  $\text{Fe}^{3+}$  with water takes place in several stages. Firstly, the iron cation reacts with water.



The resulting product will continue to bind to another water molecule.



In the final stage,



Flynn Jr. further summarized the hydrolysis processes in Fe(III) solutions at 25 °C [41]. De Bruyn et al. briefly examined the hydrolysis processes in Fe(III) solutions at 90 °C [42]. The decrease in the polymer lifetime was observed with increasing temperature, so there was precipitation rather than soluble polymers conducted by titrations at 90 °C.

## 3. Research Status of Several Key Problems in ZIRFBs

According to the characteristics of ZIRFBs, the key problems need to be improved including Fe(III) hydrolysis suppression and zinc dendrite prevention, which address the electrode, membrane, and electrolyte optimization, correspondingly.

### 3.1. Zinc Dendrite Prevention

#### 3.1.1. The 3D Electrode

The electrode is the place where zinc deposition occurs, and the structure and physical–chemical characteristics of the electrode have a critical influence on zinc plating/stripping (Z-P/S). The three-dimensional (3D) porous carbon

felts (CF) possess a high specific surface area and porosity, they can provide more sufficient spaces for Z-P/S, effectively inhibit zinc dendrites and aggregation, and ensure excellent cycle stability and rate performance [34][36].

### 3.1.2. Improving Membrane/Separator

The membrane/separator is a critical material in RFBs as well, mainly influencing the RFB performance of the battery to a great extent, especially the CE and capacity retention. The membrane/separator divides the negative and positive half-cells to refrain from battery short circuits. Meanwhile, the membrane provides ion transportation pathways to make a conductive circuit to optionally enable  $H^+$  or specific ions to pass through, avoiding the crossover between the catholyte and anolyte. To achieve a higher battery, CE requires a higher ionic selectivity of the membrane. Hence, the ideal ion-selective membranes for RFBs should satisfy the following requirements: excellent mechanical properties, high cycle stability, good ionic conductivity and selectivity, and low active species crossover and self-discharge rate. For ZIRFBs, the only concerned metallic ions which may permeate through the membranes and lead to capacity fade are  $Fe^{n+}$  and  $Zn^{2+}$ . The radius of  $Fe^{n+}$  is between 63–92 pm, which is much smaller than that of  $Zn^{2+}$  (139 pm). Hence, the crossover of  $Fe^{n+}$  takes place much easier than  $Zn^{2+}$ . It was reported that the permeability of the  $Fe^{n+}$  ion through Nafion was  $5.5 \times 10^{-5} \text{ cm}^2/\text{min}$ , which was 18.9–20.7 times higher than that of the vanadium ion ( $2.9 \times 10^{-6} \text{ cm}^2/\text{min}$ ). For the modification and improvement of membranes for RFB applications, inorganic–organic hybrid membranes and polymer blending composite membranes are widely used to reduce the undesired permeation of metallic ions and improve the ion selectivity of IEMs (ion-exchange membranes) [6][39].

The main hazard of zinc dendrites is to pierce through the membrane/separator and result in the battery short circuit. To avoid zinc dendrites from piercing the membrane/separator, membranes with high mechanical strength can be selected, such as the PBI (polybenzimidazole) membrane [34]. The PBI membrane with heterocyclic rings may ensure the rapid transportation of  $OH^-$  [34][40][43]. Concurrently, the PBI membrane owns strong mechanical stability and can resist zinc dendrites well, thus, ensuring the long-term cycling stability of alkaline ZIRFBs. At the same time, the use of porous ion-conducting membranes instead of traditional IEMs solves the problem of an increased internal resistance of the membrane due to iron ion pollution, and improves the conductivity of ions from the neutral medium through the membrane, which greatly improves the performance and stability of neutral ZIRFBs.

### 3.1.3. Adding Additives to the Electrolyte

The electrolyte is the source that affects the generation and growth of zinc dendrites. Therefore, the employment of additives into the catholyte/anolyte is a common method to suppress zinc dendrites by direct intervention in the formation of crystal nuclei. Additives can be mainly divided into three categories: metal ions, organic molecules, and polymers.

Metallic ions may influence Zn nucleation, and thus, affect the growing process. Therefore, a compact and homogeneous Zn deposit layer is obtained [44]. Zhang et al. reported [44] that the aqueous  $CaCl_2$  solution containing  $NH_4Cl$  is appropriate to be a supporting electrolyte [45]. Severe Zn dendrites are detected by SEM in 0.1 M  $ZnCl_2$

solution. Meanwhile, bulk Zn metal is detected with 1 M  $\text{NH}_4\text{Cl}$  as the supporting electrolytes. The cyclic voltammogram (CV) curves show the redox peaks sharpen obviously in the presence of  $\text{NH}_4\text{Cl}$  and independent of the amounts of  $\text{NH}_4\text{Cl}$ , meaning that the nucleation hysteresis decreases significantly. It can be confirmed that the addition of  $\text{NH}_4\text{Cl}$  may promote Z-P/S significantly. However, no prominent Zn dendrite, but only bulk Zn with random holes, is detected in the  $\text{CaCl}_2/\text{H}_2\text{O}$  (3.5 m) solution with 0.5 M  $\text{NH}_4\text{Cl}$ . The CV curves are analogous to those in aqueous  $\text{NH}_4\text{Cl}$  solutions, but the redox peak currents enhance with the addition of  $\text{NH}_4\text{Cl}$ . Therefore, for Z-P/S, a preferable supporting electrolyte has been an aqueous  $\text{CaCl}_2$  and  $\text{NH}_4\text{Cl}$  solution. The charge–discharge curves under various current densities demonstrate a clear plateau with an average voltage of 1.5 V. The CE and EE reach 94% and 75% at  $20 \text{ mA cm}^{-2}$ , respectively.

### 3.1.4. Flow Field Regulation

The electrolyte flow acts a vital role in Zn dendrites, not only owing to changing the gradient distribution of zinc ions, but also reshaping the orientation of dendritic growth. When electrolyte flow velocity is  $50 \text{ mL min}^{-1}$ , the species concentration distribution is uniformly obtained by numerical simulation [46]. It is very clear that two different zinc-depositing morphologies can be observed under the conditions of the quiescent electrolyte and the flowing electrolyte [47]. A higher flow rate of the electrolyte may enhance the transport velocity of  $\text{Zn}^{2+}$  which accelerates the diffusion process on the electrode accessory surface and the mass-transfer process in the bulk electrolyte, thus, finally reducing the  $\text{Zn}^{2+}$  concentration gradients and constraining the formation and growth of dendrites. Furthermore, a relatively high flow rate results in mitigating dendritic growth, as the formed dendrites are washed away directly by the electrolyte [17].

## 3.2. Fe(III) Hydrolysis Suppression

Both  $\text{Fe}^{2+}$  and  $\text{Fe}^{3+}$  have hydrolytic reactions in an aqueous solution. It has been reported that the hydrolysis product of iron ions will combine with the sulfonic group in the membrane to increase membrane resistance [48]. The hydrolytic reactions of  $\text{Fe}^{3+}$  are much stronger than those of  $\text{Fe}^{2+}$  and, consequently, occur at a much lower pH [49]. However, the hydrolysis of  $\text{Fe}^{3+}$  is easier to be suppressed in a hydrochloric acid environment [45][50].

In the catholyte of acidic ZIRFBs, polymerization takes place more seriously during the  $\text{Fe}^{2+}$  oxidation reaction, and ferrihydrite precipitation takes place during the  $\text{Fe}^{3+}$  hydrolysis process. The polymerization and hydrolysis reactions are rapidly promoted by enhancing  $\text{H}^+/\text{OH}^-$  ions formed due to water electrolysis. To address this issue, seven types of  $\text{Fe}^{2+}$ -complexing ligands are tested and reported, but some issues remain if its consider the binding stability and electrochemical performance of the  $\text{Fe}^{2+}$ -ligand complex [51]. It can be concluded that a novel  $\text{Fe}^{2+}$ -pyridine complexation in the catholyte has been presented for acidic ZIRFBs with a long cycle life and high performance over other  $\text{Fe}^{2+}$ -complexing ligands. In comparison to other complexing ligands, the  $\text{Fe}^{2+}$ -complexation with pyridine presents the highest electrochemical activity and reversibility [51].

## 3.3. Electrolyte Optimization

### 3.3.1. Concentration and Additives

By optimizing the composition of the electrolyte, Yuan et al. made the concentration of the  $\text{Fe}(\text{CN})_6^{3-}/\text{Fe}(\text{CN})_6^{4-}$  redox couples achieve  $1 \text{ mol L}^{-1}$ , far exceeding the previously reported concentration ( $0.4 \text{ mol L}^{-1}$ ) [34]. The high concentration of active redox couples enables the system with a high-energy density. The battery can realize 500 cycles of charge–discharge cycling under 80 and  $160 \text{ mA cm}^{-2}$ , and still maintain an EE over 80% and CE over 99% at  $160 \text{ mA cm}^{-2}$ . The results verified the outstanding stability of this system. Most important of all, the functionality of this work is further verified by assembling a kW battery stack at a capital cost of less than USD 90 per kWh.

### 3.3.2. Zinc–Bromide Complexation

To ensure the long-term operation stability of neutral ZIRFBs, Yang et al. proposed the use of  $\text{Br}^-$  ions to stabilize  $\text{Zn}^{2+}$  through complexation interactions in the neutral electrolytes [52]. The results of cyclic voltammetry indicate that the redox reversibility has been significantly enhanced between  $\text{Zn}^{2+}$  and Zn. To tackle the issue of the sluggish kinetics of the coordination interaction between  $\text{Br}^-$  and  $\text{Zn}^{2+}$ ,  $\text{ZnBr}_2$  as the electrolyte additive was directly selected to boost the process of complexation. By employing active  $\text{K}_3\text{Fe}(\text{CN})_6$  in the catholyte and modified species in the anolyte, the proposed neutral ZIRFB demonstrates excellent efficiencies and cycle stability (without obvious capacity decay) during 2000 cycles (356 h) [52].

### 3.3.3. pH

For ZIRFBs, plate electrodes or porous CFs are generally adopted for Z-P/S. During charging, zinc ions or zincate ions are continuously converted to zinc metal, and then, finally, are completely plated on the electrode. Once the deposition is finished on the electrode completely, no further electroplating will be carried out. Further charging will lead to a sharp increase in the charge potential, thus, resulting in the irreversible HER in the negative half-cell.

Liu et al. investigated the effect of several inorganic and organic additives on water migration in alkaline ZIRFBs [53]. Although all these additives are proved to be effective to suppress water migration, the organic additive, such as xylitol, sorbitol, and mannitol with several hydroxyl groups, can increase the alkalinity of the electrolyte, which in turn, accelerates the corrosion rate of zinc metal and further aggravates the HER of the battery.

### 3.3.4. Mix System

Fe–Cr RFB in the mixed electrolyte was first invented to tackle the cross-contamination issue [13]. Hybrid RFBs, such as Zn–Fe, all-Fe, Sn–Fe, have been widely explored in order to get rid of the bondage of high-cost membrane materials. Zhou et al. reported an Sn–Fe RFB, employed  $\text{SnCl}_2$  and  $\text{FeCl}_2$  as both an anolyte and catholyte, and delivered 78.5% of EE and 0.96% per cycle of the capacity decay rate at  $200 \text{ mA cm}^{-2}$  [54]. At present, a long lifetime and a high-power density of Zn–Fe RFBs are achieved through additional operation and structural design.

## Abbreviations

RFBs	redox flow batteries
ZIRFBs	zinc–iron redox flow batteries
ZBRFB	zinc-based RFB
VRFB	vanadium RFB
R.T.	room temperature
OCV	open-circuit voltage
OCP	open-circuit potential
CEM	cationic exchange membrane
IEM	ion exchange membrane
n-IEMs	non-ionic membranes
PES	poly (ether sulfone)
PEG	polyethene glycol
SPEEK-K	sulfonated polyether ether ketone
PBI	polybenzimidazole
BMImCl	1-butyl-3-methylimidazolium chloride
CF	carbon felts
Z-P/S	zinc plating/stripping
CV	cyclic voltammogram
EE	energy efficiency
CE	current efficiency
VE	voltage efficiency
HER	hydrogen evolution reaction
SOC	state of charge
MC	microporous carbon
THEED	N, N, N' N'-Tetra(2- hydroxyethyl) ethylenediamine

chnol.

Ming,  
energy

Res. 2019, 43, 1387–1410.

3. Pagliaro, M.; Meneguzzo, F. Distributed Generation from Renewable Energy Sources: Ending Energy Poverty across the World. *Energy Technol.* 2020, 8, 2000126.

4. Fernandez-Marchante, C.M.; Millán, M.; Medina-Santos, J.I.; Lobato, J. Environmental and Preliminary Cost Assessments of Redox Flow Batteries for Renewable Energy Storage. *Energy Technol.* 2020, 8, 1900914.
5. Zhang, C.; Wei, Y.-L.; Cao, P.-F.; Lin, M.-C. Energy storage system: Current studies on batteries and power condition system. *Renew. Sustain. Energy Rev.* 2018, 82, 3091–3106.
6. Sun, C.; Negro, E.; Vezzù, K.; Pagot, G.; Cavinato, G.; Nale, A.; Herve Bang, Y.; Di Noto, V. Hybrid inorganic-organic proton-conducting membranes based on SPEEK doped with WO<sub>3</sub> nanoparticles for application in vanadium redox flow batteries. *Electrochim. Acta* 2019, 309, 311–325.
7. Pal, D.; Chakraborty, S.; Chattopadhyay, S. Recent Progress in Al-, K-, and Zn-Ion Batteries: Experimental and Theoretical Viewpoints. *Energy Technol.* 2021, 9, 2100382.
8. Hu, Y.; Sun, D.; Luo, B.; Wang, L. Recent Progress and Future Trends of Aluminum Batteries. *Energy Technol.* 2019, 7, 86–106.
9. Zhang, H.; Sun, C. Cost-effective iron-based aqueous redox flow batteries for large-scale energy storage application: A review. *J. Power Sources* 2021, 493, 229445.
10. Horowitz, Y.; Schmidt, C.; Yoon, D.-H.; Riegger, L.M.; Katzenmeier, L.; Bosch, G.M.; Noked, M.; Ein-Eli, Y.; Janek, J.; Zeier, W.G.; et al. Between Liquid and All Solid: A Prospect on Electrolyte Future in Lithium-Ion Batteries for Electric Vehicles. *Energy Technol.* 2020, 8, 2000580.
11. Zhang, H.; Lu, W.; Li, X. Progress and Perspectives of Flow Battery Technologies. *Electrochem. Energy Rev.* 2019, 2, 492–506.
12. Ye, J.; Xia, L.; Wu, C.; Ding, M.; Jia, C.; Wang, Q. Redox targeting-based flow batteries. *J. Phys. D Appl. Phys.* 2019, 52, 443001.
13. Sun, C.; Zhang, H. Review of the Development of First-Generation Redox Flow Batteries: Iron-Chromium System. *ChemSusChem* 2021, 15, e202101798.
14. Esan, O.C.; Shi, X.; Pan, Z.; Huo, X.; An, L.; Zhao, T.S. Modeling and Simulation of Flow Batteries. *Adv. Energy Mater.* 2020, 10, 2000758.
15. Kim, K.J.; Park, M.-S.S.; Kim, Y.-J.J.; Kim, J.H.; Dou, S.X.; Skyllas-Kazacos, M. A technology review of electrodes and reaction mechanisms in vanadium redox flow batteries. *J. Mater. Chem. A* 2015, 3, 16913–16933.
16. Arenas, L.F.; Loh, A.; Trudgeon, D.P.; Li, X.; de León, C.P.; Walsh, F.C. The characteristics and performance of hybrid redox flow batteries with zinc negative electrodes for energy storage. *Renew. Sustain. Energy Rev.* 2018, 90, 992–1016.
17. Xu, Z.; Fan, Q.; Li, Y.; Wang, J.; Lund, P.D. Review of zinc dendrite formation in zinc bromine redox flow battery. *Renew. Sustain. Energy Rev.* 2020, 127, 109838.

18. Khor, A.; Leung, P.; Mohamed, M.R.; Flox, C.; Xu, Q.; An, L.; Wills, R.G.A.; Morante, J.R.; Shah, A.A. Review of zinc-based hybrid flow batteries: From fundamentals to applications. *Mater. Today Energy* 2018, 8, 80–108.
19. Li, Z.; Weng, G.; Zou, Q.; Cong, G.; Lu, Y.-C. A high-energy and low-cost polysulfide/iodide redox flow battery. *Nano Energy* 2016, 30, 283–292.
20. Qin, Y.; Li, X.; Liu, W. High-performance aqueous polysulfide-iodide flow battery realized by an efficient bifunctional catalyst based on copper sulfide. *Mater. Today Energy* 2021, 21, 100746.
21. Huskinson, B.; Marshak, M.; Suh, C.; Er, S.; Gerhardt, M.; Galvin, C.J.; Chen, X.; Aspuru-Guzik, A.; Gordon, R.G.; Aziz, M.J. A metal-free organic–inorganic aqueous flow battery. *Nature* 2014, 505, 195–198.
22. Chen, Q.; Gerhardt, M.R.; Hartle, L.; Aziz, M.J. A Quinone-Bromide Flow Battery with 1 W/cm<sup>2</sup> Power Density. *J. Electrochem. Soc.* 2015, 163, A5010–A5013.
23. Ulaganathan, M.; Aravindan, V.; Yan, Q.; Madhavi, S.; Skyllas-Kazacos, M.; Lim, T.M. Recent Advancements in All-Vanadium Redox Flow Batteries. *Adv. Mater. Interfaces* 2016, 3, 1500309.
24. Jiang, B.; Wu, L.; Yu, L.; Qiu, X.; Xi, J. A comparative study of Nafion series membranes for vanadium redox flow batteries. *J. Membr. Sci.* 2016, 510, 18–26.
25. Jiang, H.; Shyy, W.; Wu, M.; Zhang, R.; Zhao, T. A bi-porous graphite felt electrode with enhanced surface area and catalytic activity for vanadium redox flow batteries. *Appl. Energy* 2019, 233–234, 105–113.
26. Lu, W.; Yuan, Z.; Zhao, Y.; Li, X.; Zhang, H.; Vankelecom, I.F.J. High-performance porous uncharged membranes for vanadium flow battery applications created by tuning cohesive and swelling forces. *Energy Environ. Sci.* 2016, 9, 2319–2325.
27. Song, Y.; Li, X.; Yan, C.; Tang, A. Uncovering ionic conductivity impact towards high power vanadium flow battery design and operation. *J. Power Sources* 2020, 480, 229141.
28. Song, Y.; Li, X.; Xiong, J.; Yang, L.; Pan, G.; Yan, C.; Tang, A. Electrolyte transfer mechanism and optimization strategy for vanadium flow batteries adopting a Nafion membrane. *J. Power Sources* 2020, 449, 227503.
29. Li, T.; Xing, F.; Liu, T.; Sun, J.; Shi, D.; Zhang, H.; Li, X. Cost, performance prediction and optimization of a vanadium flow battery by machine-learning. *Energy Environ. Sci.* 2020, 13, 4353–4361.
30. Lv, Y.; Li, Y.; Han, C.; Chen, J.; He, Z.; Zhu, J.; Dai, L.; Meng, W.; Wang, L. Application of porous biomass carbon materials in vanadium redox flow battery. *J. Colloid Interface Sci.* 2020, 566, 434–443.

31. Sun, C.; Vezzù, K.; Pagot, G.; Nale, A.; Bang, Y.H.; Pace, G.; Negro, E.; Gambaro, C.; Meda, L.; Zawodzinski, T.A.; et al. Elucidation of the interplay between vanadium species and charge-discharge processes in VRFBs by Raman spectroscopy. *Electrochim. Acta* 2019, 318, 913–921.
32. Zeng, Y.; Zhao, T.; An, L.; Zhou, X.; Wei, L. A comparative study of all-vanadium and iron-chromium redox flow batteries for large-scale energy storage. *J. Power Sources* 2015, 300, 438–443.
33. Zhou, X.; Zhao, T.; An, L.; Zeng, Y.; Wei, L. Critical transport issues for improving the performance of aqueous redox flow batteries. *J. Power Sources* 2017, 339, 1–12.
34. Yuan, Z.; Duan, Y.; Liu, T.; Zhang, H.; Li, X. Toward a Low-Cost Alkaline Zinc-Iron Flow Battery with a Polybenzimidazole Custom Membrane for Stationary Energy Storage. *iScience* 2018, 3, 40–49.
35. Selverston, S.; Savinell, R.F.; Wainright, J.S. Zinc-Iron Flow Batteries with Common Electrolyte. *J. Electrochem. Soc.* 2017, 164, A1069–A1075.
36. Xie, Z.; Su, Q.; Shi, A.; Yang, B.; Liu, B.; Chen, J.; Zhou, X.; Cai, D.; Yang, L. High performance of zinc-ferrum redox flow battery with Ac<sup>-</sup>/HAc buffer solution. *J. Energy Chem.* 2016, 25, 495–499.
37. Xie, C.; Duan, Y.; Xu, W.; Zhang, H.; Li, X. A Low-Cost Neutral Zinc-Iron Flow Battery with High Energy Density for Stationary Energy Storage. *Angew. Chem. Int. Ed.* 2017, 56, 14953–14957.
38. Li, L.; Kim, S.; Wang, W.; Vijayakumar, M.; Nie, Z.; Chen, B.; Zhang, J.; Xia, G.; Hu, J.; Graff, G.; et al. A Stable Vanadium Redox-Flow Battery with High Energy Density for Large-Scale Energy Storage. *Adv. Energy Mater.* 2011, 1, 394–400.
39. Sun, C.; Negro, E.; Nale, A.; Pagot, G.; Vezzù, K.; Zawodzinski, T.A.; Meda, L.; Gambaro, C.; Di Noto, V. An efficient barrier toward vanadium crossover in redox flow batteries: The bilayer hybrid inorganic-organic membrane. *Electrochim. Acta* 2021, 378, 138133.
40. Yuan, Z.; Yin, Y.; Xie, C.; Zhang, H.; Yao, Y.; Li, X. Advanced Materials for Zinc-Based Flow Battery: Development and Challenge. *Adv. Mater.* 2019, 31, 1902025.
41. Byrne, R.H.; Yao, W.; Luo, Y.-R.; Wang, B. The dependence of Fe(III) hydrolysis on ionic strength in NaCl solutions. *Mar. Chem.* 2005, 97, 34–48.
42. Dousma, J.; De Bruyn, P. Hydrolysis-precipitation studies of iron solutions. I. Model for hydrolysis and precipitation from Fe(III) nitrate solutions. *J. Colloid Interface Sci.* 1976, 56, 527–539.
43. Nawn, G.; Pace, G.; Lavina, S.; Vezzù, K.; Negro, E.; Bertasi, F.; Polizzi, S.; Di Noto, V. Interplay between Composition, Structure, and Properties of New H<sub>3</sub>PO<sub>4</sub>-Doped PBI<sub>4</sub>N–HfO<sub>2</sub> Nanocomposite Membranes for High-Temperature Proton Exchange Membrane Fuel Cells. *Macromolecules* 2015, 48, 15–27.

44. Kim, H.-I.; Shin, H.-C. SnO additive for dendritic growth suppression of electrolytic zinc. *J. Alloy. Compd.* 2015, 645, 7–10.
45. Zhang, Y.; Henkensmeier, D.; Kim, S.; Hempelmann, R.; Chen, R. Enhanced reaction kinetics of an aqueous Zn–Fe hybrid flow battery by optimizing the supporting electrolytes. *J. Energy Storage* 2019, 25, 100883.
46. Zhang, L.; Zhang, H.; Lai, Q.; Li, X.; Cheng, Y. Development of carbon coated membrane for zinc/bromine flow battery with high power density. *J. Power Sources* 2013, 227, 41–47.
47. Wang, K.; Pei, P.; Ma, Z.; Xu, H.; Li, P.; Wang, X. Morphology control of zinc regeneration for zinc–air fuel cell and battery. *J. Power Sources* 2014, 271, 65–75.
48. Yuan, Z.; Li, X. Ion conducting membranes for aqueous flow battery systems. *Chemical Communications* 2018, 54, 7570–7588.
49. Brown, P.L.; Ekberg, C. First Transition Series Metals. *Hydrolys. Met. Ions* 2016, 499–716.
50. Huang, Q.; Wang, Q. Next-Generation, High-Energy-Density Redox Flow Batteries. *ChemPlusChem* 2015, 80, 312–322.
51. Kim, Y.; Yun, D.; Jeon, J. Performance improvement of aqueous zinc-iron flow batteries through organic ligand complexation of Fe(II)/Fe(III). *Electrochim. Acta* 2020, 354, 136691.
52. Yang, M.; Xu, Z.; Xiang, W.; Xu, H.; Ding, M.; Li, L.; Tang, A.; Gao, R.; Zhou, G.; Jia, C. High performance and long cycle life neutral zinc-iron flow batteries enabled by zinc-bromide complexation. *Energy Storage Mater.* 2022, 44, 433–440.
53. Liu, X.; Zhang, H.; Duan, Y.; Yuan, Z.; Li, X. Effect of Electrolyte Additives on the Water Transfer Behavior for Alkaline Zinc–Iron Flow Batteries. *ACS Appl. Mater. Interfaces* 2020, 12, 51573–51580.
54. Zhou, X.; Lin, L.; Lv, Y.; Zhang, X.; Wu, Q. A Sn-Fe flow battery with excellent rate and cycle performance. *J. Power Sources* 2018, 404, 89–95.

---

Retrieved from <https://encyclopedia.pub/entry/history/show/85635>